Korean J. Chem. Eng., 32(1), 104-112 (2015)
DOI: 10.1007/s11814-014-0199-8

pISSN: 0256-1115
eISSN: 1975-7220

Synthesis, structure and photocatalytic activity of calcined Mg-Al-Ti-layered double hydroxides

Khaled Hosni*,†, Omar Abdelkarim*,†, Najoua Frini-Srasra, and Ezzeddine Srasra***

*Centre National des Recherches en Sciences des Matériaux (CNRSM), Pôle Technologique de Borj Cedria, Tunisia
**Faculté des Sciences de Tunis (FST)
(*Received 11 March 2014 • accepted 13 July 2014*)

Abstract−Mg-Al-Ti layered double hydroxides (LDH), consisting of di-, tri- and tetra-valent cations with different Al^{3+}/Ti^{4+} ratio, have been synthesized by co-precipitation which was demonstrated as efficient visible-light photocatalysts. The structure and chemical composition of the compound were characterized by PXRD, FT-IR, SAA, N_2 adsorption-desorption isotherms, and DSC techniques. It is found that no hydrotalcites structure were formed for $Ti^{4+}/(Ti^{4+}+Al^{3+})>0.5$ and the substitution of Ti(IV) for Al(III) in the layer increases the thermal stability of the resulting LDH materials. The calcined sample containing titanium showed relatively high adsorption capacity for MB as compared to that without titanium. Results show that the pseudo-second-order kinetic model and the Langmuir were found to correlate the experimental data well. The photocatalytic activity was evaluated for the degradation of the methylene blue. The photocatalytic activity increased with the increase of the Al/Ti cationic ratio. 71% of the dye could be removed by the Mg/Al/Ti-LDH with the cationic ratio Al/Ti=0 : 1 and calcined at 500 °C.

Keywords: LDH, Photocatalysis, Methylene Blue, Titanium, Hydrotalcite, DRX

INTRODUCTION

Environmental contamination is a major problem threatening societies today. Industrial, agricultural and domestic wastes, due to the rapidly developing technological progress, are discharged untreated directly into the water ways corrupting rivers, lakes and oceans. While the rates of development and waste production are not likely to diminish, efforts to control and dispose of wastes are appropriately increasing.

Wastewaters from textile industries represent a serious problem all over the world. They contain different types of synthetic dyes which are known to be a major source of environmental pollution in terms of both the volume of dye discharged and the effluent composition [1]. Of the volume of wastewater containing processed textile dyes, it is estimated that 1-15% of the dye is lost in the effluents during the dyeing process and steady increasing [2]. Among 7×105 tones and approximately 10.000 different types of dyes and pigments produced worldwide, most of these dyes are toxic, mutagenic and carcinogenic. Moreover, they are very stable to light, temperature and microbial attack, making them recalcitrant compounds. From an environmental point of view, the removal of synthetic dyes is of great concern. Among several chemical, physical methods and adsorption, photocatalytic degradation is one of the effective techniques that have been successfully employed for color removal from wastewater. Anatase-type titania has been proven as environmental friendly photocatalysts because of its capability to decompose the different organic and inorganic pollutants [3,4]. Ti containing hydrotalcite have received much attention for their potential application for removal toxic anionic substances from industry wastewater [5].

Hydrotalcite is a natural layered mineral, so-called anionic clay, which constitutes a class of lamellar ionic compound. It contains a positively charged hydroxide layer and charge-balancing anions in the interlamellar space besides water molecules. A wide range of compositions are possible for synthetic hydrotalcites, based on the general formula $[M^{II}_{1-y}L^{III}_{y}(OH)_2]^{y+}[X^{n-}]_{y/n}[H_2O]_z$ where M^{II} and M^{III} are the divalent and trivalent cations in the octahedral positions within the hydroxide layers, where y can have values between 0.17 and 0.33; Xn- is an interlayer anion with a negative charge n^- [6-8], and z is the number of water molecules. Many anions or anionic complexes, both organic and inorganic, can be incorporated into the hydrotalcite structure. The reason for the potential application of hydrotalcites as catalysts rests with the ability to make mixed metal oxides at the atomic level, rather than the particle level. Such mixed metal oxides are formed through the thermal decomposition of the hydrotalcite [9]. A number of papers dealing with systems containing one divalent (Mg, Fe, Ni, Zn, Co, Mn, Cd, Ca, Cu…) and one trivalent 'Al, Fe, Ga, Cr, V, In,…) cation exist [10]. A few systems containing two divalent and one trivalent cation have been reported as precursors for mixed oxide catalysts [11]. Only a limited number of systems containing one divalent and two trivalent cations have been described [12,13]. Only Saber [14] reported that the preparation of II-IV-LDH, as Zn-Ti, Zn-Sn and Co-Ti LDH, consisting of di- and tetravalent cations, is possible.

The present study reports a simplified method to synthesize the carbonate forms of layered double hydroxides consisting of di- tri- and tetravalent cations. A series of Mg-Al-Ti-CO_3 layered double hydroxides (LDHs), with different Al/Ti molar ratio, have been syn-

†To whom correspondence should be addressed.
E-mail: hosnikhaled@gmail.com

thesized by conventional co-precipitation of magnesium, aluminum and titanium salts from homogeneous solution. The composition of the structure of the dried precipitates was investigated by infrared spectroscopy, differential scanning calorimetry (DSC) and powder X-ray diffraction. The calcined samples at 500 °C were tested for the photodegradation of methylene blue from aqueous solution.

EXPERIMENTAL

1. Sample Preparation

A series of Mg-Al-Ti-CO_3 hydrotalcite-like layered compounds have been synthesized by conventional coprecipitation method with some modifications using an aqueous solution of Na_2CO_3 as precipitant [15]. The samples were synthesized at room temperature (23±0.1 °C) by dropwise addition, under constant stirring, of a solution containing of $Mg(NO_3)_2{\cdot}6H_2O$, $Al(NO_3)_3{\cdot}9H_2O$ and $TiCl_4$ (their concentrations were varied so as to have the $Mg^{2+}/(Al^{3+}+Ti^{4+})$ molar ratio=3.0 and the Al^{3+}/Ti^{4+} molar ratio varies from 1 : 0 to 0 : 1) to another solution containing Na_2CO_3. The pH of the slurry was maintained constant at 10±0.2 by adding Na(OH) (2 N) when necessary. The slurry was subsequently aged at room temperature for 24 h. The resulting precipitates were collected by centrifugal separation and washed thoroughly with deionized water to eliminate excess Na^+ and chloride ions, followed by drying overnight at room temperature. The samples were identified as Al/Ti x : y, where x : y represents the Al/Ti molar ratio. For example, Al/Ti 9 : 1 stands for the precipitate prepared with 90% of Al^{3+} and 10% of Ti^{4+}.

2. Characterization of Materials

The dried precipitates were characterized by X-ray diffraction (XRD) to determine the species present and their degree of crystallinity. The X-ray diffractograms were obtained by using a PANalytical X'Pert HighScore Plus' diffractometer using monochromated CuKα radiation. Nitrogen adsorption measurements were performed at −196 °C with an Autosorb-1 unit (Quantachrome, USA) for the determination of sample textural properties using the multipoint Brunauer-Emmet-Teller (BET) method. The samples were out gassed at 120 °C under a vacuum at 10^{-3} mmHg for 3.5 h. Fourier-transform infrared (FT-IR) spectra were recorded as KBr pellets using a Perkin-Elmer FT-IR (model 783) instrument. KBr pellets were prepared by mixing 5 wt% anionic clay with 95 wt% KBr and pressing. Differential scanning calorimeter (DSC) experiments were performed with Mettler Toledo DSC-823 type thermal analyzer at heating rate of 20 °C·min^{-1}. The Mg, Al and Ti contents were assayed by atomic absorption spectrophotometer (AAS Vario 6).

3. Photocatalytic Reactions

The photo-degradation of methylene blue (MB) in aqueous solution using the calcined samples was carried out in a 1,000 mL Pyrex reactor under irradiation with visible-light. The visible light irradiation source was a 300 W xenon lamp equipped with a wave length pass filter with a length of 420 nm. Running water was circulated through the jacket to ensure constant temperature of the action mixture, which was stirred magnetically. Appropriate amount of catalyst (1,000 mg) was added to 1,000 mL MB solution (50 mg L^{-1}) and vigorously stirred in the dark for 120 min to reach the adsorption-desorption equilibrium before the irradiation started. Then the reaction solution was exposed to visible-light irradiation while being agitated with a magnetic stirrer. At given time intervals, analytical samples (3 mL) were taken from the reaction dispersion, followed by centrifugation to separate the solid from the liquid before measurement. The filtrates were analyzed quantitatively by measuring the absorption band maximum (669 nm) using a Hach RD/4000 UV-vis spectrophotometer. Calibration curves were constructed for MB degradation, and all experiments were performed three times to verify the repeatability of the results. The blank reaction was carried out following the same procedure without adding catalyst.

RESULTS AND DISCUSSION

1. Characterization of the Mg-Al-Ti-LDHs

1-1. X-ray Powder Diffraction

Fig. 1 illustrates the powder XRD patterns for Mg-Ti LDHs with various Al^{3+}/Ti^{4+} molar ratio in the preparation process. A strong reflection (003) was observed just for the samples prepared with Al^{3+}/Ti^{4+} molar ratio of 2 : 1, 3 : 1, 9 : 1 and 1 : 0; XRD patterns also show the reflections of (006), (012), (110) and (113), which can be indexed to typical LDH materials (PDF card N° 14-0191) [16]. The difference between these samples is in the intensity of the (00*l*) reflection. As the $Ti^{4+}/(Ti^{4+}+Al^{3+})$ molar ratio increases, from 0 to 0.5, the intensity of the reflections decreases, corresponding to an increase of the formation of the LDH structure. Above this ratio, the XRD patterns of samples show that no hydrotalcite structure is formed.

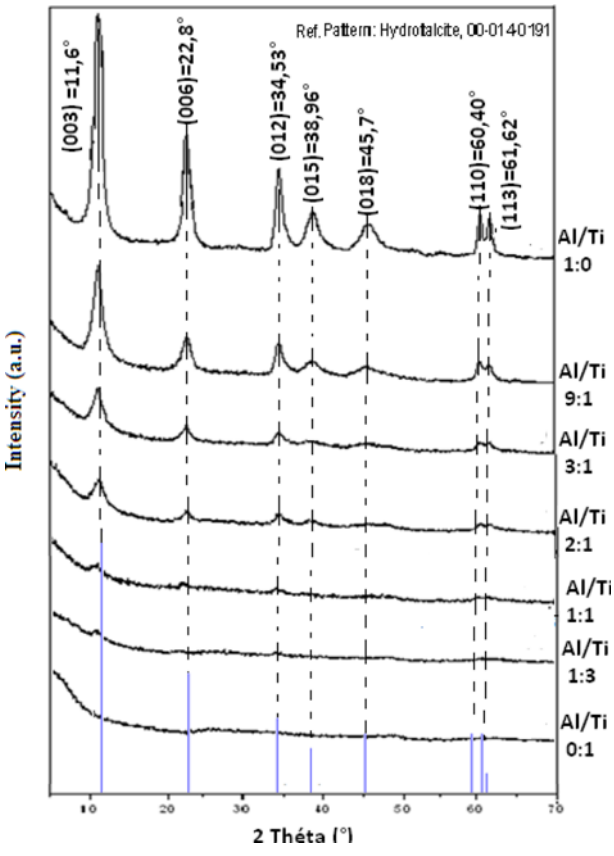

Fig. 1. X-ray diffraction pattern of uncalcined samples.

Table 1. Composition and surface area of the various solids and lattice parameters of the LDH samples

Sample	Mg : Al : Ti		Lattice parameters		Surface area $m^2 \cdot g^{-1}$	
	In solution	In solid	a (Å)	c (Å)	Before calcination	After calcination
Al/Ti 1 : 0	3.0 : 1.0 : 0	2.98 : 1.05 : 0	3,066	23,397	65,75	99
Al/Ti 9 : 1	3.0 : 0.9 : 0.1	2.94 : 0.79 : 0.09	3,068	23,490	64,99	102
Al/Ti 3 : 1	3.0 : 0.75 : 0.25	2.79 : 0.73 : 0.26	3,070	23,521	55,99	105
Al/Ti 2 : 1	3.0 : 0.67 : 0.33	2.92 : 0.65 : 0.31	3,072	23,655	48,14	109
Al/Ti 1 : 1	3.0 : 0.50 : 0.50	2.99 : 0.47 : 0.51	--	---	47,79	119
Al/Ti 1 : 3	3.0 : 0.25 : 0.75	2.83 : 0.23 : 0.76	--	--	37,09	121
Al/Ti 0 : 1	3.0 : 0.0 : 1.0	2.93 : 0.0 : 1.02	--	--	33,24	139

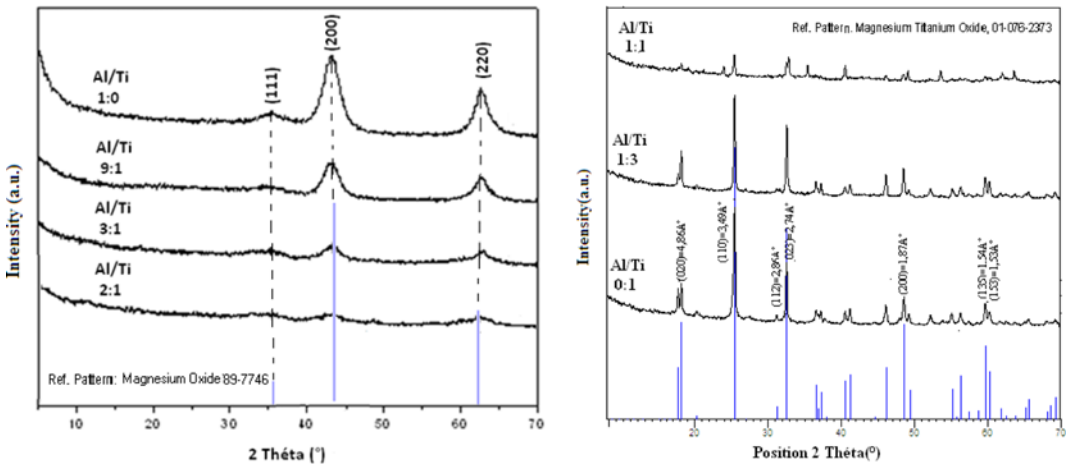

Fig. 2. The XRD pattern of the samples calcined at 500 °C.

It was found that the basal reflection ($2\theta \approx 10.8^{o}$, d_{003}=0.78 nm) of Mg-Al-Ti LDHs displayed a little shift to higher scattering angle compared with natural and synthetic carbonate-containing hydrotalcites with divalent and trivalent cations in the host layers ($2\theta \approx 11.6^{o}$, d_{003}=0.77 nm) [17,18], indicating that the basal spacing increases with the incorporation of tetravalent metal (Ti) in hydrotalcites materials. This is in accordance with the previous report on Ti-containing LDHs [19]. The increase in the interlayer distance of Mg-Al-Ti-CO_3 LDH could be attributed to the larger ion radii of Ti^{4+} than that of Al^{3+} (0.072 nm *versus* 0.052 nm).

Assuming a hexagonal crystal system, the lattice parameters were calculated from (110) and (003) reflections and are collected in Table 1. The a parameter corresponds to the cation-cation gap within the brucite layer and the c parameter is the thickness of the layer made of a brucite-like film and an interlayer. The marginal increase *of lattice parameters, a and c, in Ti-HT compared to those found* in case of Mg-Al-HT (sample noted Al/Ti 1 : 0) could be due to (i) substitution of Al^{3+} (r=0.053 nm) by the relatively larger Mg^{2+} ion (0.057 nm) as a result of lowering Al^{3+} ion equivalent to Ti^{4+} content in the precursor or (ii) partial incorporation of Ti^{4+} (r=0.072 nm) in place of Al^{3+} (r=0.053 nm) in the HT framework [20]. The latter effect caused a higher amount of CO_3^{2-} as compensating anion in the interlayer, which led to an increase of *c* parameter.

The nature of the crystalline phases generated after calcination of Ti-LDH is of interest from the viewpoint of their photocatalytic application. Fig. 2 indicates the decomposition of Mg-hydrotalcite upon calcining at 500 °C for 4 h. The XRD pattern (Fig. 2) shows that the layered structure of the original LDH is completely destroyed and indicates only MgO peaks (PDF card N° 89-7746) [21,22], suggesting an almost total decomposition of the original LDH and elimination of the most interlayer carbonate anions and water-like phases due to the collapse of layered structure. No TiO_2 phase observed shows that Ti^{4+} is dispersed in MgO rock salt phase as a solid solution. The formation of solid solution is also observed during the thermal decomposition of Mg-Al LDH [23]. However, for the samples containing a higher quantity in Ti^{4+} (samples prepared with a Al/Ti=1 : 1; 1 : 3; 0 : 1) the calcination with 500 °C gives place to the formation of a mixed oxide $MgTi_2O_5$ (PDF card N° 762373).

1-2. Element Chemical Analysis

Element chemical analysis for Mg, Al, and Ti for the samples prepared is included in Table 1. The molar Mg/(Al+Ti) ratio was in all cases reasonably close to the expected value of 3. The analytical data suggest that the Ti^{4+} is included in the composition of the brucite layer of the LDH samples.

1-3. FT-IR Spectroscopy

The FT-IR spectrum of the sample prepared with Al/Ti=0 : 1, illustrated in Fig. 3, shows a strong band centered around 3,450 cm^{-1} that is ascribed to a superposition of the OH stretching mode of layer hydroxyl groups and hydrogen-bonded interlayer water molecules. For hydrotalcite Al/Ti=1 : 0 this band appears around

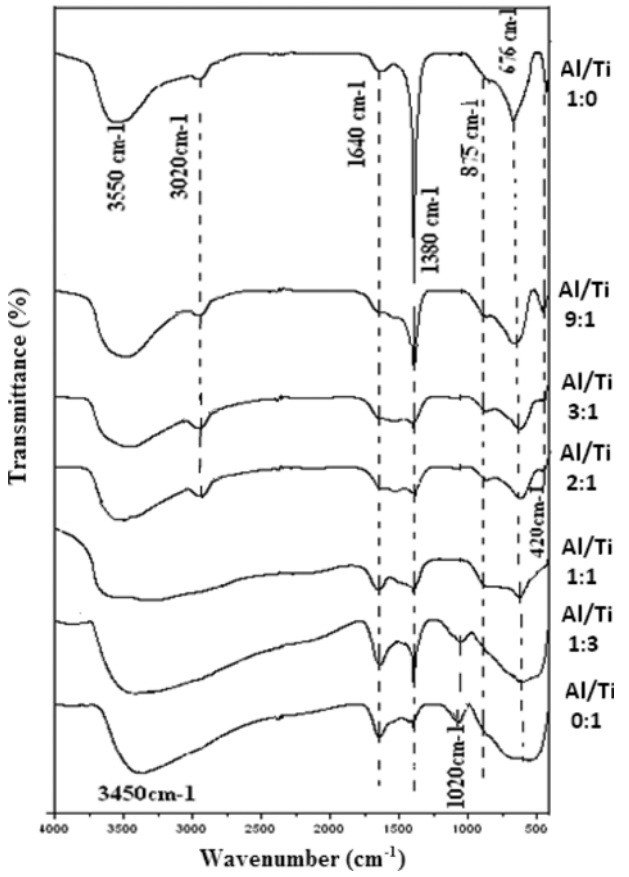

Fig. 3. FT-IR spectrum of the Mg-Al-Ti-CO_3 with different Al/Ti molar ratio.

3,550 cm^{-1}. The extreme broadness of the OH band is due to the presence of hydrogen bonding between hydroxides of layers, interlayer water and anions in the interlayer gap. The shift of OH stretching mode of layer hydroxyl groups to low frequency is probably caused by the electron density on the O-H bond modified by Ti^{4+} electro-negativity [24].

A weak shoulder band at around 3,020 cm^{-1} has been ascribed to the OH stretching mode of interlayer water molecules, hydrogen-bonded to interlayer carbonate anions [25] which appears only in the spectra of the samples prepared with Al/Ti=1 : 0; 9 : 1; 3 : 1; and 2 : 1 (samples containing a relatively small quantity of Ti^{4+}). The absence of this band for the other samples shows that no hydrotalcites were formed if $Ti^{4+}/Al^{3+}+Ti^{4+}>0.5$. This observation was confirmed by the XRD results.

The spectra of the sample prepared with Al/Ti 9 : 1 3 : 1 and 2 : 1 show a low-resolution band around 1,640 cm^{-1} ascribed to the bending mode of water molecules, which indicates a small amount of interlayer water in the samples due to abundant anions compensated positive charge of the layer.

For carbonate LDH, which consists of Mg and Al (sample Al/Ti 1 : 0), interlayer carbonate anions are symmetrically hydrogen-bonded to water molecules. Only a single band is observed at 1,380 cm^{-1}, so the symmetry of carbonate anions is close to free anions. For Mg-Al-Ti-CO_3, however, this band is split into two located at 1,509 and 1,385 cm^{-1}. The splitting is probably due to the restricted symmetry in the interlayer space. Ti^{4+} cations incorporated in the brucite-like layer bring two valence positive charges, so the electrostatic attraction between the layer and the interlayer carbonate anions is stronger than that in Mg-Al-CO_3 LDH, influencing the symmetries of the interlayer anions [26].

Bands at lower wave numbers might be due to other vibrational modes of hydrogen carbonate but more probably to vibrations implying M-O, M-O-M, and O-M-O bonds in the layers. The band between 440-420 cm^{-1} is due to the metal-oxygen vibrations in the layers and is typical of this kind of layered solids [26].

1-4. Textural Properties

Low temperature N_2 adsorption-desorption isotherms of Mg-Al-Ti-CO_3, with various molar ration of Al/Ti, show a type II isotherm (figure not shown) due to capillary condensation in mesopores where adsorption is limited for high relative pressure [27]. The isotherms were found to exhibit H3 type hysteresis loop characteristic of pores with narrow necks, which is associated with aggregates of plate-like particles giving rise to slit-shaped pores. The specific surface areas of the Mg-Al-Ti-CO_3 were determined by the single-point BET method and were included in Table 1. It was found that the values of the specific surface areas of the calcined samples were much greater than the values obtained for their precursors at the precursor temperature at 120 °C. It was suggested that a porous system was developed in the calcined sample during the transfor-

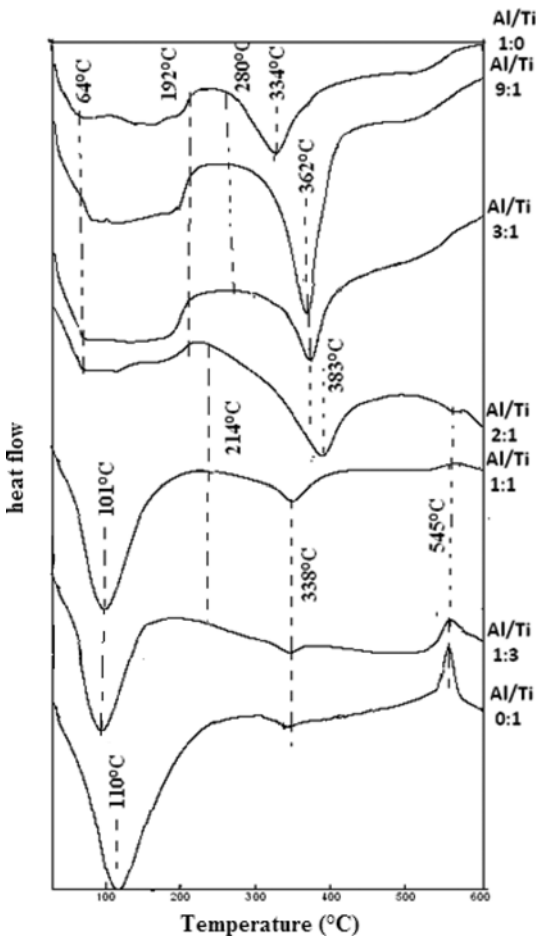

Fig. 4. DSC of the Mg-Al-Ti hydrotalcite.

mation of CO_3^{2-} to CO_2 [28].

1-5. Thermal Analysis: Differential Scanning Calorimetry

Minerals such as the synthesized hydrotalcites decompose at low temperatures and lend themselves to differential scanning calorimetry. Fig. 4 displays the analyses of the Mg/Al/Ti hydrotalcites, clearly showing that the thermal decomposition is complex with many overlapping peaks. It is convenient to subdivide the data in accordance with the temperature range: (a) steps below 200 °C, (b) steps from 200 to 300 °C, (c) and steps above 300 °C. For the Al/Ti=1 : 0 sample two predominant heat flow steps are observed at 64 and around 192 °C. These two heat flow steps are attributed to adsorbed water and to interlayer water [29]. The higher temperature heat flow steps observed at around 334 °C are assigned to the loss of hydroxyls from the structure. Upon substitution of the Al by Ti, this heat flow step passes to 383 °C when $Ti^{4+}/(Ti^{4+}+Al^{3+})$ molar ratio increases from 0 to 0.5, indicating that the introduction of titanium improves the thermal stability of hydrotalcite. This behavior can be explained as follows: the interlayer carbonate ions, initially arranged parallel to the brucite layers, are arranged perpendicular to the layers following the introduction of titanium ions. This shift can be explained by the strong interaction titanium-carbonate. This behavior was observed by Saber, 2008 [30]. The hypothesis of arrangement switching carbonate ions is already justified by the evolution of the parameter *c* previously calculated.

For samples prepared with ratios of $Ti^{4+}/Al^{3+}+Ti^{4+}\geq 0.5$, the DSC curves show two endothermic transitions observed at 100 °C and 383 °C corresponding to the departure of the adsorbed water and the dehydroxylation of the compound. The low intensity of the second transition is probably due to the absence of carbonate ions in the structure. The exothermic peak observed at 545 °C, is attributed to the formation of the $MgTi_2O_5$ compound previously identified by XRD.

2. The Adsorption Study

Since photocatalysis requires an adsorption step, we studied the adsorption of methylene blue on the surface of the different photocatalysts. All solutions were prepared and stocked in polyethylene flasks. All sorption experiments were performed in 50 ml polyethylene tubes. Stock solution of MB (500 mg·l^{-1}) was prepared and suitably diluted to the required initial concentrations. Adsorption experiments were at room temperature (around 25 °C) under batch mode [31].

The time-dependent sorption of dye on calcined hydrotalcite was carried out with 50 mg of the adsorbent and 30 ml of 30 mg l^{-1} dye solution. The mixtures were stirred at low speed (~100 rpm) for different time intervals (0.25-4 h). After separating the turbidity by centrifugation, the final concentration of dye (C_f) of MB was obtained by measuring O.D. at 669 nm using a Hach RD/4000 UV-vis spectrophotometer.

The adsorption isotherms were obtained by the batch equilibrium technique. One hundred milligrams of adsorbent was weighed in polyethylene tubes and then these were filled with 30 ml of aqueous solutions of MB ranging in concentration from 0 to 100 mg·l^{-1}. The mixtures were stirred for 2 h at room temperature, centrifuged and the supernatant dye concentrations were determined.

The samples were filtered prior to analysis to minimize interference of the carbon fines with the analysis. Each experiment was duplicated under identical conditions. Blanks containing no dye were used for each series of experiments as controls. The amount of adsorption at equilibrium, Q_e (mg g^{-1}), was calculated by

$$Q_e = \frac{(C_0 - C_e)\times V}{w}$$

where C_0 and C_e (mg·l^{-1}) are the liquid-phase concentrations of dye at initial and equilibrium, respectively. V is the volume of the solution, and w is the mass of adsorbent used (g).

To express the results of experimental adsorption measurements in the form of one or more equilibrium adsorption isotherm theories, the Langmuir isotherm and the Freundlich isotherm theories were tested in this study since they have been widely applied and found to be effective to describe many adsorption processes.

Only the samples prepared with Al/Ti molar ratio 0 : 1; 1 : 0; 1 : 1 and 9 : 1 were used for the MB photocatalytic degradation.

2-1. The Effect of Contact Time

The sorption rate gives important information for designing batch sorption systems. Information on the kinetics of solute uptake is required for selecting optimum operating conditions (time) for photo-catalytic process. Fig. 5 shows the plot of MB sorption, by calcined hydrotalcite prepared with various Al/Ti molar ratios, versus contact time. For all the samples, the sorption was found to be rapid at the first period of the process and then the rate of sorption was slower and stagnated with the increase in contact time. The equilibrium time was 60 min. This time must be taken into account before carrying out the catalytic application. But to ensure itself of the establishment of the equilibrium adsorption, the contact time was fixed at 2 hours.

To characterize the kinetics involved in the process of the MB adsorption, on the calcined hydrotalcite, the pseudo-first-order [32] and the pseudo-second-order [33] rate equations were proposed. The conformity between experimental data and the model predicted values was expressed by the correlation coefficients (R^2, values close or equal to 1). A relatively high R^2 value indicates that the model successfully describes the kinetics of MB adsorption.

2-1-1. The Pseudo First-order Equation

The pseudo first-order equation is generally expressed as fol-

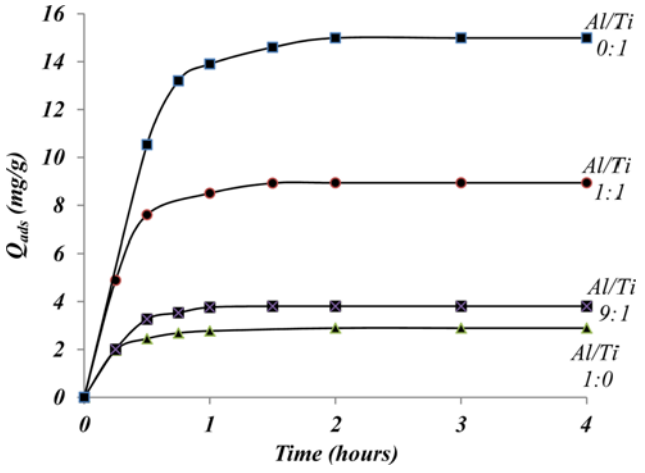

Fig. 5. Effect of time of contact for the adsorption of MB on the samples calcined.

lows [32]:

$$\frac{dq_t}{q_1(t)} = k_1 \times (q_e - q_t) \quad (1)$$

where q_e and q_t are the adsorption capacity at equilibrium and at time t, respectively ($mg \cdot g^{-1}$), k_1 is the rate constant of pseudo first-order adsorption (h^{-1}). After integration and applying boundary conditions the Eq. (1) becomes:

$$\frac{1}{q_1(t)} = \frac{k_1}{q_1} \times \left(\frac{1}{t}\right) + \frac{1}{q_1} \quad (2)$$

2-1-2. The Pseudo Second-order Equation

The pseudo second-order adsorption kinetic rate equation is expressed as [33]:

$$\frac{dq_t}{q_1(t)} = k_2 \times (q_e - q_t)^2 \quad (3)$$

where k_2 is the rate constant of pseudo second-order adsorption ($g \cdot mg^{-1} \cdot h^{-1}$).

For the boundary conditions t=0 to t=t and q_t=0 to q_t=q_t, the integrated form of Eq. (3) becomes:

$$\frac{1}{(q_1 - q_t)} = \frac{1}{q_e} + k_2 t \quad (4)$$

which is the integrated rate law for a pseudo-second-order reaction.

Eq. (4) can be rearranged to obtain Eq. (5), which has a linear form:

$$\frac{t}{q_t} = \frac{1}{k_2 q_2^2} + \frac{t}{q_e} \quad (5)$$

The plot of (t/q_t) and t of Eq. (5) should give a linear relationship from which q_e and k_2 can be determined from the slope and intercept of the plot, respectively.

The obtained parameter data and the correlation coefficients, R^2, are given in Table 2. The table shows that the correlation coefficients for the pseudo-second-order kinetic model are closer to one than that of the Lagergren first order. From these results it was concluded that the pseudo-second-order model was better than the Lagergren first-order for the systems investigated in this work. Since dye adsorption follows pseudo-second-order kinetics, this suggested that boundary layer resistance was not the rate-limiting step [34]. The rate of dye adsorption may be controlled largely by a chemisorption process.

2-2. Adsorption Isotherms

Equilibrium adsorption isotherms are of fundamental importance in the study of adsorption systems since they indicate how

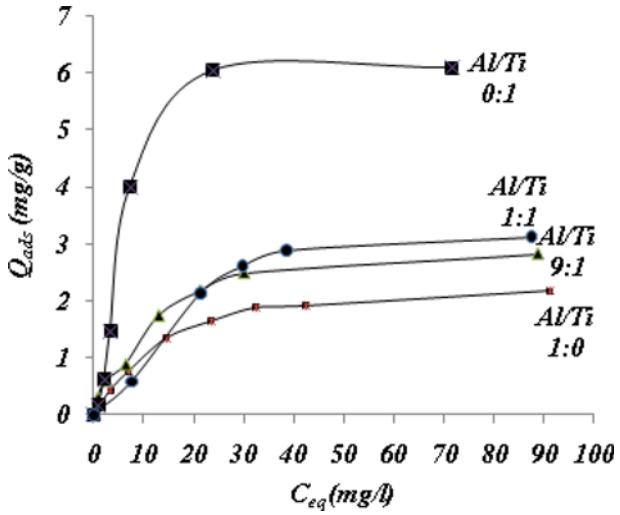

Fig. 6. Adsorption of MB by the calcined samples.

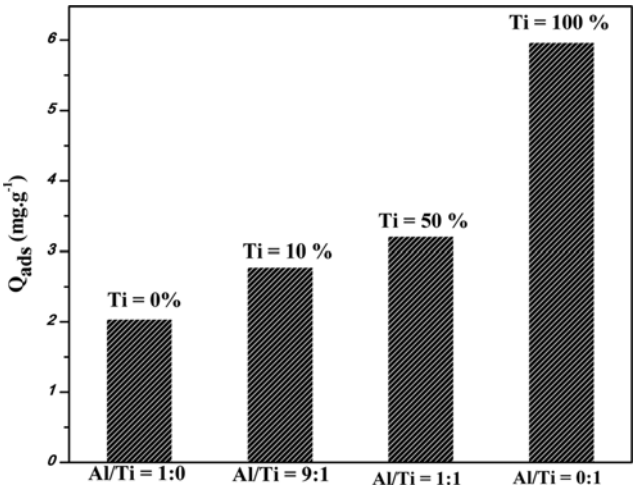

Fig. 7. The MB sorption capacity as a function of Ti^{4+} content.

the MB partitions themselves between the medium and liquid phase with increasing concentration at equilibrium. When medium and MB solutions are contacted, the concentration of the dye on the medium will increase until a dynamic equilibrium is reached, at which point there is a defined distribution of dye species between the solid and liquid phases. The adsorption isotherms were constructed using the batch equilibrium technique, where a fixed mass of adsorbent was agitated with methylene blue solution of various concentrations for a sufficient length of time to ensure that equi-

Table 2. Kinetic constants for MB adsorption onto calcined hydrotalcites

Sample	First-order			Pseudo-second-order		
	k_1 (h^{-1})	q_1 (mg/g)	R_1^2	k_2 ($mg/g^{-1}h^{-1}$)	q_2 (mg/g)	R_2^2
Al/Ti=1 : 0	0,1352	3,081	0,985	3,568	2,977	0,999
Al/Ti=9 : 1	0,283	4,502	0,9000	2,270	3,958	0,999
Al/Ti=1 : 1	0,254	10,193	0,937	0,840	9,319	0,998
Al/Ti=0 : 1	0,1929	16,778	0,895	2,440	15,720	0,999

Table 3. Langmuir and Freundlich isotherm constant for sorption of MB dye by Mg-Al-Ti-LDH

Sample	Langmuir parameters			Freundlich parameters		
	Q_M	K_L	R^2	K_f	1/n	R^2
Al/Ti=1 : 0	2.551	0.070	0.994	1.113	0.147	0.978
Al/Ti=9 : 1	3.184	0.090	0.991	1.255	0.183	0.870
Al/Ti=1 : 1	3.580	0.082	0.994	1.072	0.248	0.821
Al/Ti=0 : 1	8.080	0.054	0.746	2.490	0.307	0.723

librium had been achieved. An agitation time of 4 h and equilibrium temperature of 25 °C were used. Sorption isotherms of MB by calcined LDH are shown in Fig. 6. It is evident that MB adsorption capacity increases with the incorporation of tetravalent metal (Ti) in hydrotalcites materials (Fig. 7). For example, at a similar MB concentration, sorption capacity of Al/Ti=0 : 1 was greater three times than that of Al/Ti=1 : 0 LDH.

Isotherms for MB sorption by Mg-Al-Ti-LDH were modeled by two commonly used isotherm equations, Langmuir (Eq. (6)) [35] and Freundlich (Eq. (7)) [36].

$$\frac{1}{Q_{ad}} = \frac{1}{Q_M K_L} \times \frac{1}{C_{eq}} + \frac{1}{Q_M} \tag{6}$$

$$Q_{ad} = K_f \times (C_{eq})^{1/n} \tag{7}$$

where Q_e ($mg \cdot g^{-1}$) is the amount of MB sorbed at equilibrium, Q_M ($mg \cdot g^{-1}$) the theoretical maximum monolayer sorption capacity, C_e ($mg \cdot L^{-1}$) the equilibrium concentration of MB in solution, and K_f, n and K_L are empirical constants. The calculated Langmuir and Freundlich isotherm constants are given in Table 3. The table indicates that the best fit was obtained by the Langmuir model. This model is based on the assumption that sorption takes place at specific homogeneous sites within the adsorbent. Once a dye molecule occupies a site, no further adsorption can take place at that site, and only a monolayer is formed at the maximum adsorption.

3. Photodegradation of MB by Sample Calcined

The photocatalytic activity of calcined Mg-Al-Ti-LDH is shown in Fig. 8. The photodegradation of MB was under irradiation with visible-light (420 nm). A mixture of 1 liter of MB (50 $mg \cdot L^{-1}$) solution and 1 g of catalyst was vigorously stirred in the dark for 120 min to establish an adsorption/desorption equilibrium. Then the solution was stirred under visible-light irradiation for photocatalytic reaction. The decomposed percentage of MB was calculated by the absorbance intensity of the sample at time intervals. The strong absorption bands of MB located at λ=669 nm decreased gradually upon increasing irradiation time, and the absorbance of dyes solution was became constant after 120 min of irradiation for all the calcined Mg-Al-Ti-LDH catalyst (Fig. 8). In addition, the solution color changed from an initial deep blue to nearly transparent during the degradation process of MB. Taking into account the important role of Ti in the photocatalysis, the results of the influence of molar ratio of Al/Ti on its photocatalytic are shown in Fig. 8. It was found that all the Mg-Al-Ti-LDHs with 9 : 1; 1 : 1; and 0 : 1

Table 4. Pseudo-first order constants and photodegradation rates of MB for different photocatalysts

Sample	Photodegradation rate	Pseudo-first-order	
		K_{app}	R^2
Al/Ti=1 : 0	3%	0.0387	0.9953
Al/Ti=9 : 1	18%	0.0783	0.9993
Al/Ti=1 : 1	42%	0.1375	0.9807
Al/Ti=0 : 1	71%	0.3079	0.9777

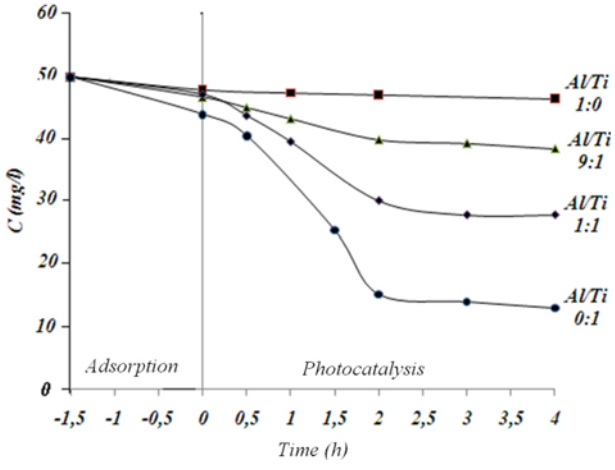

Fig. 8. Photodegradation and adsorption of MB vs irradiation time under visible-light irradiation (λ>420 nm) with the presence of different photocatalysts.

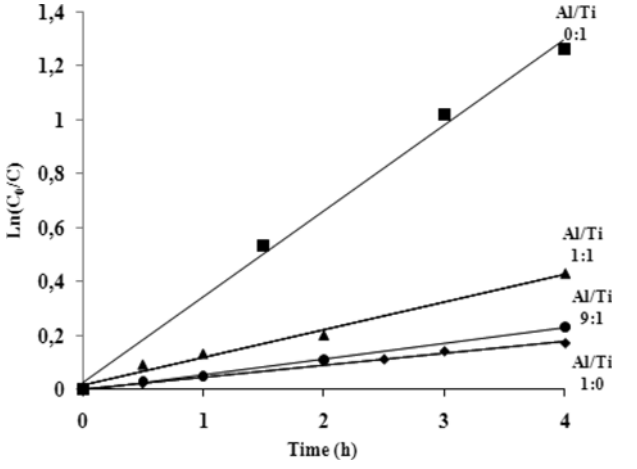

Fig. 9. Layouts of Ln (C_0/C) according to time of irradiation for methylene blue (where C and C_0 are the MB concentration at time intervals and initial state, respectively).

displayed high photocatalytic activity under visible-light irradiation. The decomposition of MB by the Ti-LDH (Al/Ti=0 : 1) reaches 71% over 180 min, comparative to 42% and 18% by the samples with Al/Ti=1 : 1 and 9 : 1, respectively (Table 4).

As shown in Fig. 9, the plots of $\ln(C_0/C)$ vs irradiation time suggest that the photodegradation of MB follows the pseudo-first-order rate law (Fig. 8) [37]. The rate constant was calculated to be 0.3079 min^{-1} with Mg-Al-Ti LDH (Al/Ti=0 : 1) as the photocatalyst, much larger than that of Mg-Al-Ti LDH (Al/Ti=1 : 0) (Table 4).

The high photocatalytic performance of the Mg-Al-Ti-LDH can be explained by the octahedral coordination of Ti atoms in the brucite-like sheets. It is well-known that light absorption by the material and the migration of the light induced electrons and holes are the most key factors controlling a photocatalytic reaction, which is relevant to the electronic structure characteristics of the material [38]. Moreover, in addition, the high photocatalytic activity of the calcined Mg-Al-Ti-LDH is also attributed to its hierarchical structure and high specific surface (99-139 $m^2 \cdot g^{-1}$). The high specific surface area is responsible for providing strong adsorption ability toward target molecules and thus the generation of photo-induced electron-hole pairs of active sites [39,40]. The long-period performance of the Mg-Ti-LDH (Al/Ti=0 : 1) was also tested (curves not shown); the photocatalyst is stable under four repeated application cycles with nearly constant photodecomposition percentage, indicating that Mg-Al-Ti LDH does not deactivate during the photocatalytic process of the pollutant molecules. Moreover, this material can be easily separated from the reaction system due to the microscopic particle size of Mg-Ti LDH. The results thus indicate that the Mg-Ti-LDH can be used as an attractive photocatalyst for large-scale environmental purification with high photocatalytic activity, long-term sustainability and excellent recyclability.

CONCLUSION

Mg-Al-Ti LDH was prepared by co-precipitation, which displayed isomorphous substitution of the Ti^{4+} in the brucite layer.

The calcination of precursors at 500 °C yielded mixed oxides with poorly crystalline MgO and $MgTi_2O_5$ type structures, which can be fully reconstructed to original LDH on rehydration at ambient temperature and atmospheric pressure. The introduction of Ti^{4+} in the lattice significantly influenced the surface area, and the adsorption capacity of the MB. The Mg-Al-Ti hydrotalcites displayed superior photocatalytic activity in the visible part of the solar spectrum for the degradation of MB compared with Mg-Al-LDH. The remarkable visible-light photocatalytic activity of calcined Ti-LDH is attributed to its hierarchical microsphere structure as well as high specific surface. In addition, Mg-Al-Ti LDH retained its activity after several recycles of the MB photodegradation. Therefore, it is expected that the Mg-Al-Ti LDH with hierarchical structure in this work can be potentially used as an effective and recyclable visible-light photocatalyst for large-scale environmental purification.

ACKNOWLEDGEMENTS

The authors wish to express their gratitude to the Laboratory of Physical Chemistry of Mineral Materials and their Applications, National Research Center for Materials Science, High Technology Borj Cedria - Tunisia.

REFERENCES

1. P. C. Vandevivere, R. Bianchi and W. Verstraete, *Review of Emerging Technologies, J. Chem. Technol. Biotechnol.*, **72**, 289 (1998).
2. H. Zollinger, Color Chemistry, VCH, Weinheim, 2nd Ed. (1991).
3. L. Joon-Yeob and J. Wan-Kuen, *Environ. Eng. Res.*, **17**(4), 179 (2012).
4. L. Kumaresan, B. Palanisamy, M. Palanichamy and V. Murugesan, *Environ. Eng. Res.*, **16**(2), 81 (2011).
5. N. Das and A. Samal, *Micropor. Mesopor. Mater.*, **72**, 219 (2004).
6. R. Allmann, *Acta Crystallogr. Sect. B*, **24**, 972 (1986).
7. S. Miyata, *Clays Clay Miner.*, **23**, 369 (1975).
8. H. F. W. Taylor, *Miner. Mag.*, **39**, 377 (1973).
9. M. Valcheva-Traykova, V. Davidova ans A. Weiss, *J. Mater. Sci.*, **28**, 2157 (1983).
10. F. Cavani, F. Trifiro and A. Vaccari, *Catal. Today*, **11**, 173 (1991).
11. F. Kooli, K. Kosuge and A. Tsunashima, *J. Mater. Sci.*, **30**, 4591 (1995).
12. F. Kooli, K. Kosuge and A.Tsunashima, *J. Solid State Chem.*, **118**, 4591 (1995).
13. J. M. Fernandez, C. Barriga, M. A. Ulibarri, F. M. Labajos and V. Rives, *Chem. Mater.*, **9**, 312 (1997).
14. O. Saber and H. Tagaya, *J. Incl. Phenom. Macrocyclic Chem.*, **45**, 109 (2003).
15. W. T. Reichle, *J. Catal.*, **94**, 547 (1985).
16. O. Saber and H. Tagaya, *J. Inclusion Phenom.*, **45**, 17 (2003).
17. F. Leroux, M. Adachi-Pagano, M. Intissar, S. ChauvieÁre, C. Forano and J. P. Besse, *J. Mater. Chem.*, **11**, 105 (2001).
18. C. Busetto, G. Del Piero and G. Manara, *J. Catal.*, **85**, 260 (1984).
19. W. H. Zhang, X. D. Guo, J. He and Z. Y. Qian, *J. Eur. Ceram. Soc.*, **28**, 1623 (2008).
20. X. Shu, W. Zhang, J. He, F. Gao and Y. Zhu, *Solid State Sci.*, **8**, 634 (2006).
21. E. L. Crepaldi, J. Trondo, L. P. Ardoso and J. B. Valim, *J. Colloid Surf. A: Physicochem. Eng. Aspects*, **211**, 103 (2002).
22. Y. You, H. Zhao and G. F. Vance, *J. Appl. Clay Sci.*, **21**, 217 (2002).
23. W. T. Reichle, *Solid State Ionics*, **22**, 713 (1986).
24. K. T. Ehlsissen, A. Delahaye-Vidal, P. Genin, M. Figlarz and P. Willmann, *J. Mater. Chem.*, **3**, 883 (1993).
25. N. Das and A. Sandal, *Micropor. Mesopor. Mater.*, **72**, 219 (2004).
26. M. J. Hernández-Moreno, M. A. Ulibarri, J. L. Rendon and C. Serna, *J. Phys. Chem. Miner.*, **12**, 34 (1985).
27. K. S. W. Sing, D. H. Everett, R. A. W. Haul, L. Moscou, R. Pierotti, J. Rouquerol and T. Sieminiewska, *Pure Appl. Chem.*, **57**, 603 (1985).
28. W. T. Reichle, S. Y. Kang and D. S. Everhardt, *J. Catal.*, **101**, 352 (1986).
29. D. Tichit, N. Das, B. Coq and R. Durand, *Chem. Mater.*, **14**, 1530 (2002).
30. O, Saber and H, Tagaya, *J. Mater. Chem. Phys.*, **108**, 449 (2008).
31. N. Kannan, *Indian J. Environ. Protec.*, **11**(7), 514 (1991).
32. S. Lagergren, *Handlingar*, **24**(4), 139 (1898).
33. L. C. Ho, G. Rudnick, H. W. Rix, J. C. Shields, H. Daniel, D. H. McIntosh, A. V. Filippenko, W. L. W. Sargent and M. Eracleous, *Astrophysical. Journal*, **541**, 120 (2000).

34. Y. S. Ho and G. McKay, *Process Biochem*., **34**, 451 (1999).
35. I. Langmuir, *Chem. Soc*., **40**, 1361 (1918).
36. H. M. F. Freundlich, *Phys. Chem*., **57**, 385 (1906).
37. N. Barka, A. Assabbane, A. Nounah, A. Albourine and Y. Ait-Ichou, *Sciences Technologie*, **B27**, 09 (2008).
38. H. B. Fu, C. S. Pan, W. Q. Yao and Y. F. Zhu, *J. Phys. Chem*., **B109**, 22432 (2005).